Antenna integrated quantum cascade laser switchable via telecommunications wavelength probe beam

Kohoutek, John, Bonakdar, Alireza, Dey, Dibyendu, Gelfand, Ryan, Hassani Nia, Iman, et al.

John Kohoutek, Alireza Bonakdar, Dibyendu Dey, Ryan Gelfand, Iman Hassani Nia, O. Gokalp Memis, Vala Fathipour, Hooman Mohseni, "Antenna integrated quantum cascade laser switchable via telecommunications wavelength probe beam," Proc. SPIE 8456, Nanophotonic Materials IX, 845606 (15 October 2012); doi: 10.1117/12.929721

SPIE.

Event: SPIE NanoScience + Engineering, 2012, San Diego, California, United States

Antenna integrated quantum cascade laser switchable via telecommunications wavelength probe beam

John Kohoutek, Alireza Bonakdar, Dibyendu Dey, Ryan Gelfand, Iman Hassani Nia, O. Gokalp Memis, Vala Fathipour, Hooman Mohseni

Bio-Inspired Sensors and Optoelectronics Laboratory (BISOL), EECS, Northwestern University, 2145 Sheridan Rd., Evanston, Illinois, USA

ABSTRACT

Here we present an antenna-integrated QCL which can be actively and optically modulated using light in the near infrared, creating an optical nanocircuit – coupling two different frequency antennas with a nonlinear active switching element. For our design, we chose two cross-polarized bow-tie antennas with an aligned central spot. We have used detailed FDTD simulations to choose the length of each bow-tie. The larger bow-tie antenna is resonant with the QCL at 6.1 μm wavelength and is aligned perpendicular to the active region of the device because QCL emits TM polarized light. The smaller bow-tie is resonant with the incoming modulating light at 1550 nm and is aligned perpendicularly to the first bow-tie. There is a rectangular region of amorphous germanium below the smaller bow-tie which acts as an absorber at 1550 nm. When light at 1550 nm is incident upon the device, it is focused and enhanced by the smaller bowtie, creating a region of large absorption in the germanium rectangle below. Free carriers are generated, shorting the larger bow-tie which is already focusing and enhancing light from the QCL mode. When the bow-tie arms of the larger bow-tie are shorted by these free carriers, the focusing and enhancement of the light by the larger bow-tie of the QCL mode is severely diminished, affecting the entire laser output, even the far field. Simulation results, fabrication details, and finally experimental results are discussed. Such an all-optical switch could be useful for telecommunications, free space communications, or rangefinding applications.

Keywords: QCL, all optical switch, plasmonics, broadband antenna, optical nanocircuit

1. INTRODUCTION

Recently, there has been increasing activity in using SP-based devices for optical modulation and switching [1-4]. Methods of all-optical switching have become more attractive recently in integrated communications devices. Recent interest in optical force [5, 6] has even led to optical force based switching devices [4, 7]. Recent methods include use of a silicon-based MDM channel with subwavelength slits for optical source and drain to create a SP based optical modulator [1]. Another method uses a grating for the path of a SP and modulated the signal using a polymer loaded with photochromic molecules [2]. Others have shown theoretically that ultrafast and compact all-optical switches can be realized by means of a semiconductor gap-loaded nanoantenna [3]. Here we show an experimental realization of a near-field enhanced semiconductor gap-loaded nanoantenna, creating an optical nanocircuit [8] – coupling two different frequency antennas with a nonlinear active switching element. This method allows for switching of a 6.1 μm beam with a telecommunications wavelength switch beam,

The quantum cascade laser (QCL) is a unipolar semiconductor laser that works on the principle of intersubband transitions [9]. This laser is a compact semiconductor based laser source that emits light in the mid to far infrared. The cavity mode is highly sensitive to the reflectivity of the facets [10, 11], which gives an attractive method for modulation of the far field optical mode. There has also been recent increased interest in making plasmonic devices integrated with

Nanophotonic Materials IX, edited by Stefano Cabrini, Taleb Mokari, Proc. of SPIE Vol. 8456, 845606 · © 2012 SPIE · CCC code: 0277-786/12/$18 · doi: 10.1117/12.929721

quantum-cascade lasers [12-15]. Some of these devices may be used for biosensing [14, 15], as many important molecules have vibrational resonance in the terahertz [16]. In addition, plasmonic integrated QCL devices can be used for laser beamshaping or steering [17].

We have previously performed modulation of laser light in the mid-wave infrared (MWIR, 6.1 μm) by a near-field interaction at the hot spot of a plasmonic nanoantenna [11]. In this manuscript, a similar concept will be shown, which is a type of infrared switchable plasmonic quantum cascade laser in which the far field light is modulated by a near-field interaction by light at 1.55 μm. To achieve this, we used cross-polarized bow-tie antennas and a centrally located photonic absorber: a germanium nano-slab (see Figure 1). The smaller bow-tie antenna focuses the short infrared wavelength light into the gap region where the germanium is placed. We have shown previous focusing of bow-tie and other structures into subwavelength "hot spots" as is done here [5, 14, 15]. When the light is focused by the small bow-tie, the intensity is enhanced, creating a large absorption in the small volume of germanium. As a result, free carriers are generated inside the germanium, and it becomes lossy. The free charge dampens the electric field in the germanium, which is in the center of the larger bow-tie, and is where the largest change in field intensity is observed in the simulations (see Figure 2). Because the plasmonic mode of the antenna structure is strongly coupled to the cavity mode of the laser and thus affects the reflectivity of the facet, the changing of the plasmonic mode thus affects the entire output of the laser.

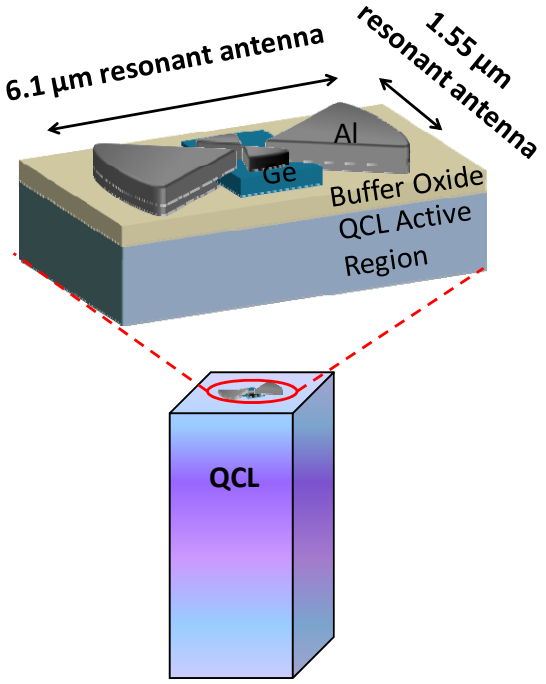

Figure 1 - Device concept, showing cross-polarized bow-tie antennas on facet of QCL. Larger bow-tie is resonant with QCL output wavelength, smaller bow-tie is resonant with switch beam. Germanium absorber is placed underneath gap region.

2. DEVICE DESIGN AND SIMULATION

The antenna structure is placed on the front facet of the QCL so that we may focus the 1550 nm switch beam on the antenna and record the 6.1 μm signal out of the back facet of the laser as in our previous set-ups [8, 11, 14, 15, 18]. We have chosen bow-ties over previous nanorod and coupled nanorod antenna designs [14, 15] because bow-ties resonate over a larger spectral range. They also offer an empty central region where a nonlinear photonic absorber may be placed. The larger bow-tie antenna is resonant with the QCL at 6.1 μm wavelength and is aligned perpendicular to the active region of the device. The output electric field of the QCL is aligned with the long axis of the larger bow-tie. The smaller bow-tie is resonant with the incoming modulating light at 1550 nm and is aligned perpendicular to the first bow-tie. There is a rectangular region (500 nm long, 250 nm wide, and 80 nm tall) of amorphous germanium below the smaller bow-tie which acts as an absorber at 1550 nm. The bow-ties are made out of a single layer of aluminum so as to avoid metal diffusion into the germanium layer below the smaller bow-tie antenna. There is a buffer layer of MgF_2 below the entire structure to insulate the top and bottom contacts of the laser as well as to protect the facet of the laser.

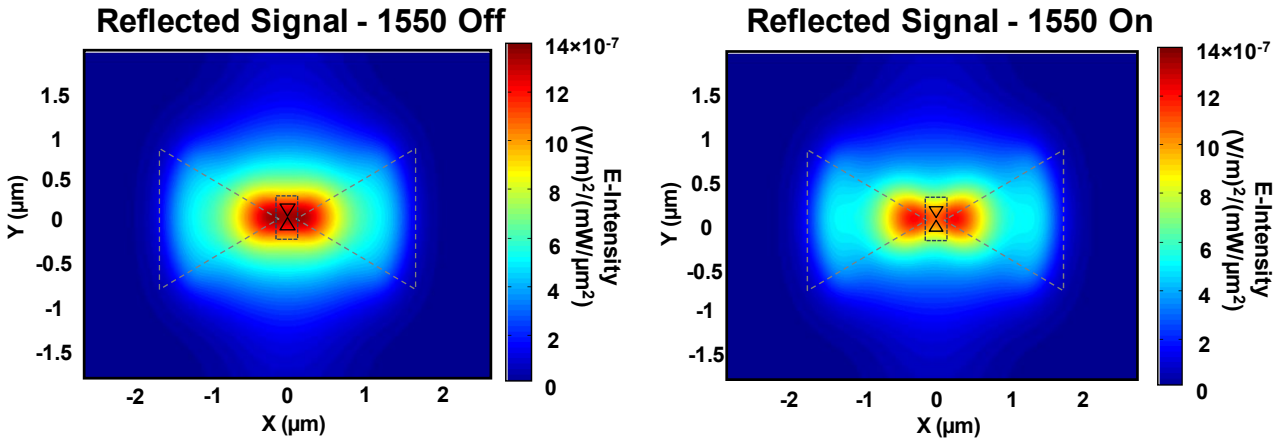

Figure 2 – Left) Simulated reflected E-Intensity signal near the antenna when 1550 nm probe signal is turned off.

(Right) – Simulated reflected E-Intensity signal near the antenna when 1550 nm probe signal is turned on

To analyze and optimize our design, we simulated the structure using three-dimensional FDTD software. All material data used in the simulation, other than the laser region, is from reference [19]. For all simulations, a truncated planewave is used. To optimize the design, a volume monitor is placed in the common gap region of the two antennas in order to calculate the average electric field intensity (E-intensity) as a function of arm length. With this method, the resonance length of the smaller antenna is found in the absence of the larger antenna. Then, the resonance length of larger antenna is found in the presence of the smaller antenna with the previously obtained resonance length. Finally, the resonance length of smaller antenna is found in the presence of larger antenna with the previously obtained resonance length. Perfectly matched layer (PML) boundary conditions are used for all the simulations. In order to find the optically induced plasma in the Ge slab, we have simulated the power absorption in the Ge for a given source intensity at 1.55 μm. Using the Drude model, the free carrier concentration and subsequently the refractive index of Ge at 6.1 μm wavelength is obtained as a function of 1.55 μm wavelength input optical power used in the experiment. Using the modified refractive index, the depth of modulation, which is defined as the ratio of power reflectivity of the QCL when the probe signal is turned on to when the probe signal is turned off, is calculated (see reflected signal plotted in Figure 2). The free carrier lifetime τ is considered as a fitting parameter in the equation $\Delta N=\Delta P=G*\tau$ where ΔN and ΔP are the change in carrier concentrations and G is the generation rate [20], to derive the same depth of modulation as demonstrated in the experimental results. Using this method, we have found the free carrier lifetime to be ~15 ns. In the literature, carrier

lifetime in Ge can vary drastically, from ms time scales in bulk Ge [21] to hundreds of nanoseconds for amorphous Si:Ge alloys [22] or even near µs for amorphous Ge [23, 24] or ~5 ns for evaporated poly-crystalline Ge [25]. We do, however, expect our experimentally determined lifetime to be on the lower end of this broad spectrum due to its amorphous nature, large surface to volume ratio, and presence of metal on the surface. Figure 4 shows the good agreement that this model achieves compared to the measured experimental data, with a single adjustable parameter – the carrier lifetime. Figure 4a shows the depth of modulation versus input power while Figure 4b shows the depth of modulation versus switch beam polarization. Figure 5a shows agreement with the frequency response of the small antenna and the final device with no adjustable parameter. We have also done a detailed simulation of our multiple quantum well structure and calculated the absorption of the structure in the near-infrared (NIR) to rule out the possibility that the absorption in the NIR may be causing a change in the intensity of the output at 6.1 µm. These simulations do show absorption nearing 10^5 m^{-1}, however, only for wavelengths below 1.2 µm for TE polarization and 1.1 µm for TM polarization. At 1550 nm, the absorption for TE and TM polarization is on the order of 10^{-2} m^{-1} and 10^{-4} m^{-1} respectively.

3. FABRICATION AND EXPERIMENT

After designing, simulating, and optimizing our structure, we have fabricated the test structure on the facet of a QCL. The QCL used in the device is the same as the one used in reference [26], with injector. After cleaving, the laser was mounted on a c-mount, and the laser facet was coated in an electron-beam evaporation chamber with layers of MgF_2/Ge. Next, focused ion beam milling (FIB) was used to mill out the isolated Ge rectangle on which the smaller bow-tie antenna would eventually sit. Next, another e-beam evaporation was done to deposit an aluminum layer. Finally, the antenna structure was milled out of the aluminum using a two-step process in FIB: first the smaller antenna aligned to the germanium rectangle was milled using a low current (9.7 pA), then the large antenna was aligned to the smaller antenna and milled at a high current (93 pA). The laser was tested at each possible stage during fabrication. The final antenna design is shown in Figure 3 (right).

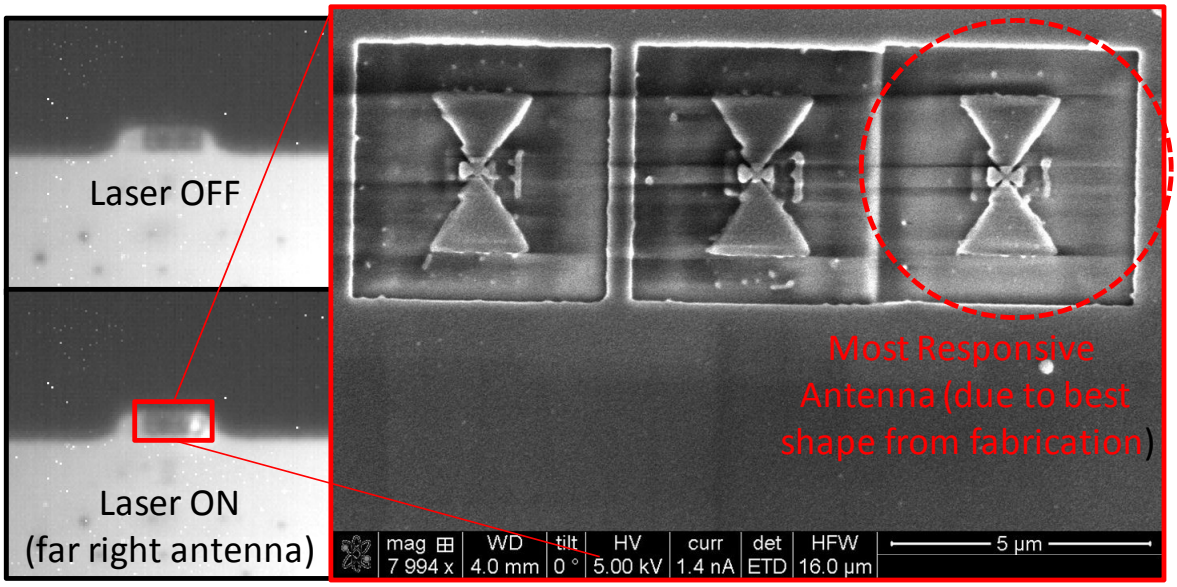

Figure 3 – Infrared image (left) showing laser spot on right side (right antenna) and SEM image (right) showing final fabricated device, rightmost antenna has best geometrical fabrication qualities.

We have constructed a two-way microscope setup for testing and characterization of the device. From the top of the setup, there is an NIR camera allowing one to view the laser facet and simultaneously focus the modulation (1550

nm wavelength) laser light onto the laser facet. From the bottom of the setup, there is a broadband inverted microscope coupling the light from the laser facet to a visible camera and mercury-cadmium-telluride (MCT) detector, allowing simultaneous viewing of the bottom facet of the laser and focusing of the beam of the QCL onto the MCT detector. We have constructed three antenna devices on the facet of the QCL, as shown in Figure 3. When the beam is focused on the rightmost device the highest change in signal is observed. We believe that the basis for this comes from the geometrical characteristics of the device. The rightmost device has the best characteristics among the three and would lead to the highest enhancement of light at 1550 nm, and therefore the highest absorption in the germanium.

We first observed the signal from the MCT detector on the oscilloscope with the 1550 nm source off and recorded its signal. Subsequently, we turned the 1550 nm source on and recorded the output of the MCT detector on the oscilloscope. When the 1550 nm source is on, there is a nearly 15% decrease in the peak signal of the QCL output. We have further characterized the device through a sideband measurement method by modulating the 1550 nm laser at 200 Hz and recording the output of the MCT detector in an RF spectrum analyzer. As the QCL is operating in pulsed mode at 0.5% duty cycle (103 kHz, 50 ns pulse width), we observe a main peak at 103 kHz. When the 1550 laser is on, we observe two sidebands at ±200 Hz with respect to the main peak. We have recorded the amplitude of the signal in dBm on the spectrum analyzer and converted it to a linear scale in Watts to observe the effect of the 1550 nm light on the modulation of the mid-infrared output of the QCL. We have varied the 1550 nm switch beam laser power, measured the output depth of modulation, and plotted the result in Figure 4a. It can be found through the Drude model that $\varepsilon_{6.1} \propto I_{1.55}^2$, where $\varepsilon_{6.1}$ is the permittivity at 6.1 μm and $I_{1.55}$ is the light intensity at 1.55 μm. Using the above relation in our FDTD simulation, we observe a quadratic relationship between depth of modulation and $I_{1.55}$. This is in concert with the experimental data (Figure 4a). We have also varied the polarization of the switch beam at 1550 nm. Figure 4b shows well matched results between the measured power and the expected $\sin^2\theta$ relationship (where θ is the angle between the incident electric field and the long axis of the bow-tie as shown in Figure 1). This is due to the cross polarization relationship between the incoming switch beam and the smaller resonant bow-tie polarization axis. We believe that the nonzero experimental signal observed at zero degrees polarization is due to experimental artifacts, such as imperfect shape of the bow-tie (different from simulation), surface roughness at all interfaces, and imperfect alignment. All of these factors could create plasmonic enhancement greater than zero at zero degrees polarization. Finally, we have varied the switch beam wavelength around 1550 nm, and recorded the output depth of modulation On the right axis, we have plotted the intensity enhancement of the smaller bow-tie given that the resonance of the smaller bow-tie is the main factor in the frequency response of the device. The simulation and experimental data agree well, both peaking near 1580 nm. Figure 5b shows the difference in signal on the oscilloscope when the switch beam is switched on. A difference in magnitude of 1.25 mV is obtained, in reference to a "before" signal of ~8 mV. This accounts for a depth of modulation of ~15%, with an input switch power of 70 $\mu W/\mu m^2$. The length of the pulse is ~50 ns, limited by heating in the laser core that is operated at 103 kHz for a 0.5% duty cycle. In Figure 4a-b, the power of modulation (left axis) is partly limited by the duty cycle and total power output of the QCL. It is also limited by the responsivity of the MCT detector used in the setup.

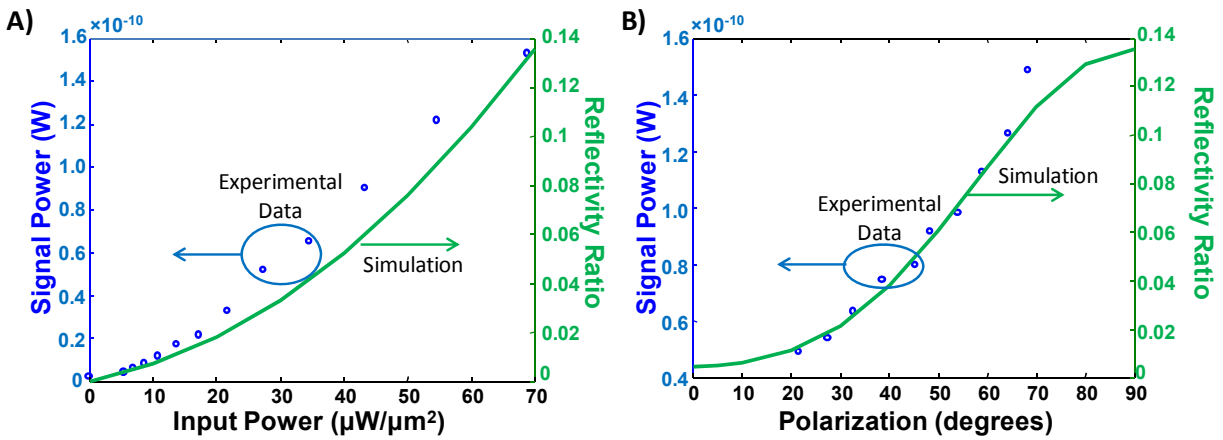

Figure 4 - (A) Sideband power versus power of 1550 nm modulation signal. Left axis shows experimental signal power, right axis shows simulation data. Experimental signal power (left axis in a-b) is limited by duty cycle and total power output, also it is reduced by the responsivity of MCT detector. (B) Sideband power versus polarization of 1550 nm modulation signal. Left axis shows experimental signal power, right axis shows simulation data.

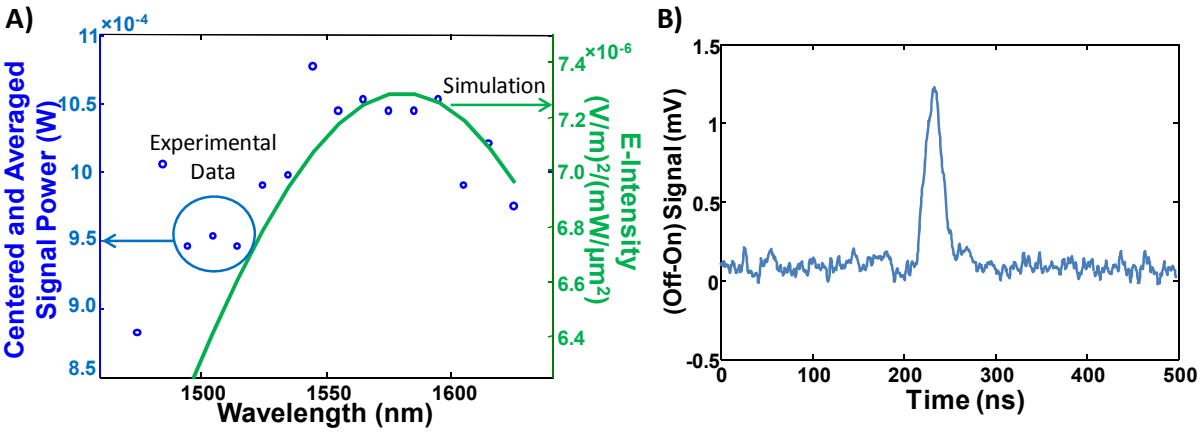

Figure 5 - (A) Sideband power versus wavelength of modulation signal. Data is centered and averaged over several measurements. Left axis shows experimental signal power, right axis shows simulation data. (B) Time response of modulated signal, showing difference in [Off] minus [On] states. [Off] nominal peak is near 8 mV, so depth of modulation is nearing 15 percent.

4. DISCUSSION AND CONCLUSION

We have considered different recombination mechanisms that are proportional to first, second, and third powers of free carrier density [27] (e.g.: Shockley-Read-Hall, radiative, and Auger recombination). In bulk single-crystal germanium, the linear term is dominant up to carrier densities of $N \sim 0.5\times10^{19}$ cm^{-3} [21]. Therefore, we first assumed the linear term is dominant in our experiment and calculated the density that fits our experimental results. The resulted value is about 1×10^{19} cm^{-3} at a carrier lifetime of about 15 ns. Considering the large surface effect in our submicron Ge piece, and the fact that it is amorphous, we think the linear term is certainly dominant. It also produces a very good fit to our experimental data (see Figure 4a).

We have observed a maximum modulation depth of ~15% at the maximum power of 70 μW/μm^2. This results in a switching energy of 8.4 pJ, in line with other all-optical switches [2, 3]. One way to improve the modulation depth would be to use a pulsed laser, which would allow for a higher carrier density. Lastly, by reducing the volume of the germanium to cover only the volume beneath the smaller bow-tie hotspot, rather than the entire area below the smaller bow-tie, we could increase the depth of modulation. This would create a higher carrier density because the carriers would have less volume to diffuse over and the loss would increase, which would increase the change in the optical properties of the larger antenna when switched.

In conclusion, we have designed, simulated, fabricated, and experimentally characterized a QCL with an integrated nonlinear optical antenna, which is switchable via a telecommunications wavelength laser. This device shows a viable optical method to modulate the far field of a laser through a near-field interaction, as in our previous device [11]. We have characterized the device for optical power, polarization, and wavelength dependence. We have determined that the effect is not due to absorption in the quantum wells. This device is a realization of an optical nanocircuit – coupling two different frequency antennas with a nonlinear active switching element. Because of the wide-ranging usefulness for terahertz and short-wave infrared laser modulators, we believe such a device could be very useful in many applications from telecommunications [28] and free space communications [29] to range-finding [30].

5. REFERENCES

[1] J. A. Dionne, K. Diest, L. A. Sweatlock, and H. A. Atwater, "PlasMOStor: A Metal-Oxide-Si Field Effect Plasmonic Modulator," Nano Letters, 9(2), 897-902 (2009).

[2] R. A. Pala, K. T. Shimizu, N. A. Melosh, and M. L. Brongersma, "A nonvolatile plasmonic switch employing photochromic molecules," Nano Letters, 8(5), 1506-1510 (2008).

[3] N. Large, M. Abb, J. Aizpurua, and O. L. Muskens, "Photoconductively Loaded Plasmonic Nanoantenna as Building Block for Ultracompact Optical Switches," Nano Letters, 10(5), 1741-1746 (2010).

[4] A. Bonakdar, J. Kohoutek, D. Dey, and H. Mohseni, "Optomechanical Nanoantenna," Optics Letters, (2012).

[5] J. Kohoutek, D. Dey, A. Bonakdar, R. Gelfand, A. Sklar, O. G. Memis, and H. Mohseni, "Opto-mechanical force mapping of deep subwavelength plasmonic modes," Nano Letters, 11(8), 3378-82 (2011).

[6] G. Volpe, R. Quidant, G. Badenes, and D. Petrov, "Surface plasmon radiation forces," Physical Review Letters, 96(23), (2006).

[7] D. Van Thourhout, and J. Roels, "Optomechanical device actuation through the optical gradient force," Nature Photonics, 4(4), 211-217 (2010).

[8] J. Kohoutek, A. Bonakdar, R. Gelfand, D. Dey, I. H. Nia, V. Fathipour, O. G. Memis, and H. Mohseni, "Integrated All-Optical Infrared Switchable Plasmonic Quantum Cascade Laser," Nano Letters, 12(5), 2537-2541 (2012).

[9] J. Faist, F. Capasso, D. L. Sivco, C. Sirtori, A. L. Hutchinson, and A. Y. Cho, "QUANTUM CASCADE LASER," Science, 264(5158), 553-556 (1994).

[10] H. C. Liu, and F. Capasso, [Intersubband Transitions in Quantum Wells: Physics and Device Applications II] Academic Press, San Diego(2000).

[11] J. Kohoutek, D. Dey, A. Bonakdar, R. Gelfand, V. Fathipour, O. G. Memis, and H. Mohseni, "Mechanical frequency and amplitude modulation of quantum cascade laser integrated with plasmonic nanoantenna," Small, (2012).

[12] N. Yu, E. Cubukcu, L. Diehl, M. A. Belkin, K. B. Crozier, F. Capasso, D. Bour, S. Corzine, and G. Hofler, "Plasmonic quantum cascade laser antenna," Applied Physics Letters, 91(17), (2007).
[13] N. Yu, E. Cubukcu, L. Diehl, D. Bour, S. Corzine, J. Zhu, G. Hoefler, K. B. Crozier, and F. Capasso, "Bowtie plasmonic quantum cascade laser antenna," Optics Express, 15(20), 13272-13281 (2007).
[14] D. Dey, J. Kohoutek, R. M. Gelfand, A. Bonakdar, and H. Mohseni, "Quantum-cascade laser integrated with a metal-dielectric-metal-based plasmonic antenna," Optics Letters, 35(16), 2783-2785 (2010).
[15] D. Dey, J. Kohoutek, R. M. Gelfand, A. Bonakdar, and H. Mohseni, "Composite Nano-Antenna Integrated With Quantum Cascade Laser," Ieee Photonics Technology Letters, 22(21), 1580-1582 (2010).
[16] M. Tonouchi, "Cutting-edge terahertz technology," Nature Photonics, 1(2), 97-105 (2007).
[17] N. Yu, R. Blanchard, J. Fan, Q. J. Wang, C. Pfluegl, L. Diehl, T. Edamura, S. Furuta, M. Yamanishi, H. Kan, and F. Capasso, "Plasmonics for Laser Beam Shaping," Ieee Transactions on Nanotechnology, 9(1), 11-29 (2010).
[18] J. Kohoutek, D. Dey, R. Gelfand, A. Bonakdar, and H. Mohseni, "An apertureless near-field scanning optical microscope for imaging surface plasmons in the mid-wave infrared," Proceedings of SPIE-The International Society for Optical Engineering. 8097-63(2010).
[19] D. Palik, [Handbook of Optical Constants of Solids] Academic, (1985).
[20] N. W. Ashcroft, and N. D. Mermin, [Solid State Physics] Brooks Cole, United States(1976).
[21] M. E. Levinshteĭn, S. L. Rumyantsev, and M. Shur, [Handbook Series on Semiconductor Parameters: Si, Ge, C (Diamond), GaAs, GaP, GaSb, InAs, InP, InSb] World Scientific, (1996).
[22] D. S. Shen, J. P. Conde, V. Chu, and S. Wagner, "CARRIER LIFETIME IN AMORPHOUS-SEMICONDUCTORS," Journal of Applied Physics, 75(11), 7349-7355 (1994).
[23] H. Watakabe, T. Sameshima, H. Kanno, and M. Miyao, "Electrical properties for poly-Ge films fabricated by pulsed laser annealing," Thin Solid Films, 508(1-2), 315-317 (2006).
[24] S. Ishii, M. Kurihara, T. Aoki, K. Shimakawa, and J. Singh, "Photoluminescence in high-quality a-Ge : H," Journal of Non-Crystalline Solids, 266, 721-725 (2000).
[25] L. Colace, G. Masini, and G. Assanto, "Ge-on-Si approaches to the detection of near-infrared light," Ieee Journal of Quantum Electronics, 35(12), 1843-1852 (1999).
[26] D. Dey, W. Wu, O. G. Memis, and H. Mohseni, "Injectorless quantum cascade laser with low voltage defect and improved thermal performance grown by metal-organic chemical-vapor deposition," Applied Physics Letters, 94(8), (2009).
[27] J. O. Drumm, B. Vogelgesang, G. Hoffmann, C. Schwender, N. Herhammer, and H. Fouckhardt, "Temperature and carrier density dependence of Auger recombination in a 3.4 mu m InAs/GaSb/AlSb type-II laser device," Semiconductor Science and Technology, 17(10), 1115-1122 (2002).
[28] D. K. Hunter, and D. G. Smith, "NEW ARCHITECTURES FOR OPTICAL TDM SWITCHING," Journal of Lightwave Technology, 11(3), 495-511 (1993).
[29] P. Boffi, D. Piccinin, D. Mottarella, and M. Martinelli, "All-optical free-space processing for optical communication signals," Optics Communications, 181(1-3), 79-88 (2000).
[30] T. Ruotsalainen, P. Palojarvi, and J. Kostamovaara, "A wide dynamic range receiver channel for a pulsed time-of-flight laser radar," Ieee Journal of Solid-State Circuits, 36(8), 1228-1238 (2001).